

# Ibn Al-Haitham Journal for Pure and Applied Sciences

Journal homepage: jih.uobaghdad.edu.iq PISSN: 1609-4042, EISSN: 2521-3407 IHJPAS. 2025, 38(4)



# Study of the Properties of Image Formation by an Optical System Consisting of a Diffractive Lens



<sup>1,2</sup>Department of Physics, College of Education for pure science (Ibn Al-Haitham), University of Baghdad, Baghdad, Iraq.
\*Corresponding Author

Received: 16 April 2025 Accepted: 29 Jun 2025 Published: 20 October 2025

doi.org/10.30526/38.4.4144

#### **Abstract**

Diffractive lenses form images based on the principle of light diffraction, unlike conventional lenses that rely on the phenomenon of refraction to form images. Diffractive lenses consist of precisely aligned structures of holes or slits that act as optical gratings. They are arranged to give the lens the optical property of changing the path of incident rays, creating an image pattern similar to that of conventional lenses. This work aims to study the image characteristics formed by diffractive lenses by conducting a computer simulation in the Zemax optical design software. The analysis tools available in the software are then used to study the quality of the resulting image and evaluate the performance of the diffractive lens. The results show that the image characteristics formed by diffractive lenses are similar to those of conventional lenses. These results indicate the image-forming performance of diffractive lenses. This gives designers flexibility in lens design, in terms of the type and number of slits used without the use of spherical surfaces.

**Keywords:** Diffractive lens, Zemax program, Point spread function, Optical transfer. function.

#### 1.Introduction

Using diffractive elements to redirect light is a promising approach for creating an image pattern similar to that of conventional optical systems with regular lenses. The diffraction pattern depends on the deflection of light as a wave when it passes through a rim, hole, or slit. This is possible in the optical element by placing systematically arranged grooves or holes on the optical element. The optical element used can be opaque, such as a type of metal interspersed with a series of holes or slits to produce diffraction. Alternatively, it can be transparent, such as dielectric materials like glass or plastic, which contain grooves or holes (1, 2).

The materials used in lens manufacturing vary depending on the type of optical system and its purpose. Transparent dielectric materials are often used in the manufacture of both diffractive and conventional lenses. Due to their abundance, light weight, ease of molding, and their suitable thermal and optical properties, they are suitable for use in both optical and non-imaging systems (3-5). Glass or plastic also has a suitable refractive index to direct refracted or incident rays to their appropriate location in the image plane. Considering that

their light absorption rate is so low that it can be neglected, this is very useful for maintaining the light intensity coming from the source to the image plane (6-8). Using gratings in optical elements produces images with special one-dimensional symmetry or radial symmetry in the image plane, such as using a cylindrical or circular Fresnel lens, which has gratings in the form of parallel lines or concentric circular gratings. Using fine holes in a diffractive lens produces a diffraction pattern with images with properties similar to those of conventional lenses (9, 10).

The Zemax optical design software was used to simulate the diffractive lens used in this research. This software provides great geometric flexibility in design due to its wide range of optical parameters. Zemax also offers a wide range of optical analysis tools to evaluate the performance of the optical system, contributing to an accurate description of image quality. These tools include macroscopic tools such as the spot diagram, or mathematical tools such as the point spread function and optical path difference (11, 12).

#### 2.Materials and Methods

Zemax software program provides a diffractive lens model using a binary system. This model divides the fine components of the lens into a binary system that allows or blocks light from passing through the lens. This simulates a diffractive lens with tiny holes. The optical parameters listed in **Table 1** were used for the design. There are five surfaces in the optical system: the first represents the light source, the second is a virtual surface that directs light rays toward the lens, and the third and fourth surfaces represent the diffractive lens surfaces, which have values ( $r_1$ =14.760,  $r_2$ =-12.226) to make the lens biconvex. The use of convexity in the lens helps direct rays better than a flat surface in this type of lens, meaning it additionally directs rays to accommodate the diffraction of rays through the lens holes. The final surface represents the image surface. The lens thickness (1 mm) was used to match the corresponding optical dimensions of the image dimension and the virtual surface dimension (13-16).

PMMA was used for the lens material due to its suitable optical properties for the design, such as its refractive index (1.49), high transparency, high hardness, and relatively large coefficient of thermal expansion compared to other transparent materials. PMMA is easy to mold during the manufacturing process, which helps produce a lens that matches the designed model. This material is prepared in a liquid form during casting, which allows for high precision in the molding process.

Zemax program does not provide a macro image of the holes in the diffractive lens, as shown in **Figure 1**, but rather provides a ready-made design for a binary system lens that allows light to pass through one location (hole = 1) or prevents light from entering another (barrier = 0). This is similar to how a compact disc (CD) reflects or transmits light depending on the location of the rays falling on the CD's sectors, which contain grooves that allow or prevent light from passing through (17-21).

The pupil diameter of the diffractive lens was used to match the other optical dimensions of the optical system (D=5mm). The diameter of the pupil determines the amount of light entering the optical system, i.e., the amount of light flux reaching the lens, which in turn determines the amount of light intensity reaching the image surface and consequently affects the clarity of the image.

A visible light source consisting of the three main wavelengths (0.486, 0.588, 0.656  $\mu$ m) was used to demonstrate the effect of chromatic aberration on an image through the phenomenon

of diffraction. The suitability of different types of wavelengths for use in diffractive lens optical systems was also investigated (22-25).

A variable field of view was used to determine the impact of the angle of incidence on image quality. The angle of incidence varies at values ( $\theta$ =0°, 5°, 10°, 15°) in only one axis (Y axis) to determine the effect of the source's deviation from the optical axis on image quality, considering the object off-axis. Displacing an object from the optical axis generates asymmetrical aberrations, such as coma aberration or astigmatism. The value and type of aberration vary depending on the object's position off-axis and the type and shape of the lens, i.e., the type of material (refractive index) and the radii of curvature (focal length) (25-30).

<b>Table 1.</b> Optical	parameters of the diffractive	ve lens in Zemax program.

Su	rf: type	[ Radius	Thickness]	Material	Clear Semi-Dia	Mech Semi-Dia
OBJ	Standard	Infinity	Infinity		Infinity	Infinity
1	Standard	Infinity	30.000		13.669	13.669
2	Binary2	14.760	1.000	PMMA	2.661	2.661
3	Standard	-12.226	12.854		2.511	2.661
IMA	Standard	Infinity	-		6.345	6.345

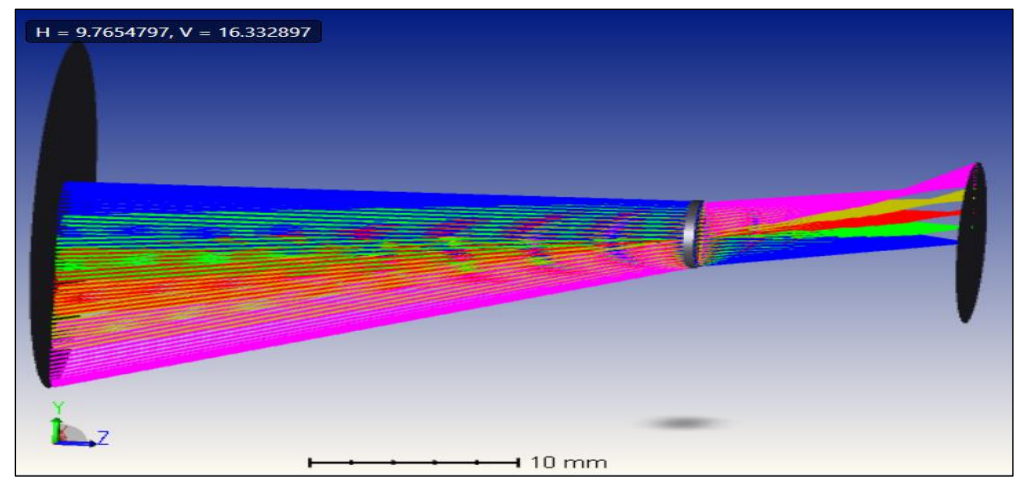


Figure 1. Layout of the optical system including a diffractive lens.

#### 3.Results

A set of image analysis tools provided by the Zemax software was used to evaluate the performance of the optical system by measuring image quality. Various tools were used in this study, each varying in approach by providing a visual, mathematical, or graphical description of the image, and evaluating it using well-known optical criteria such as the Strehl criterion, the Airy disk, or the optical transition function. A set of images was taken for each wavelength used and for each incidence angle range to determine the effect of these factors on image quality.

The point spread function PSF describes the amount of radiation distribution in the image plane in three dimensions. This tool provides a visual description for evaluating image quality by describing the distribution of rays of a point object in the image plane, whether the pattern is three-dimensional or two-dimensional. The Airy disk criterion can be used to determine image quality. If the rays are distributed within the disk by (80%), an image is considered good.

Changing the angle of incidence causes the rays to deviate from their normal path, which results in asymmetric aberration in the image and clearly changes the distribution of the rays in **Figure 2**. In the ideal case (field angle 0), the central peak disappears, and a group of secondary peaks is produced, distributed in the image plane. Thus, the central intensity

decreases, leading to a change in the features of the image. The greater the angle of incidence of the rays, the less intense the secondary peaks become, and they are distributed over a larger area in the image plane. This is due to the appearance of spherical, coma, and astigmatism aberrations in the image, resulting from the source being off-axis.

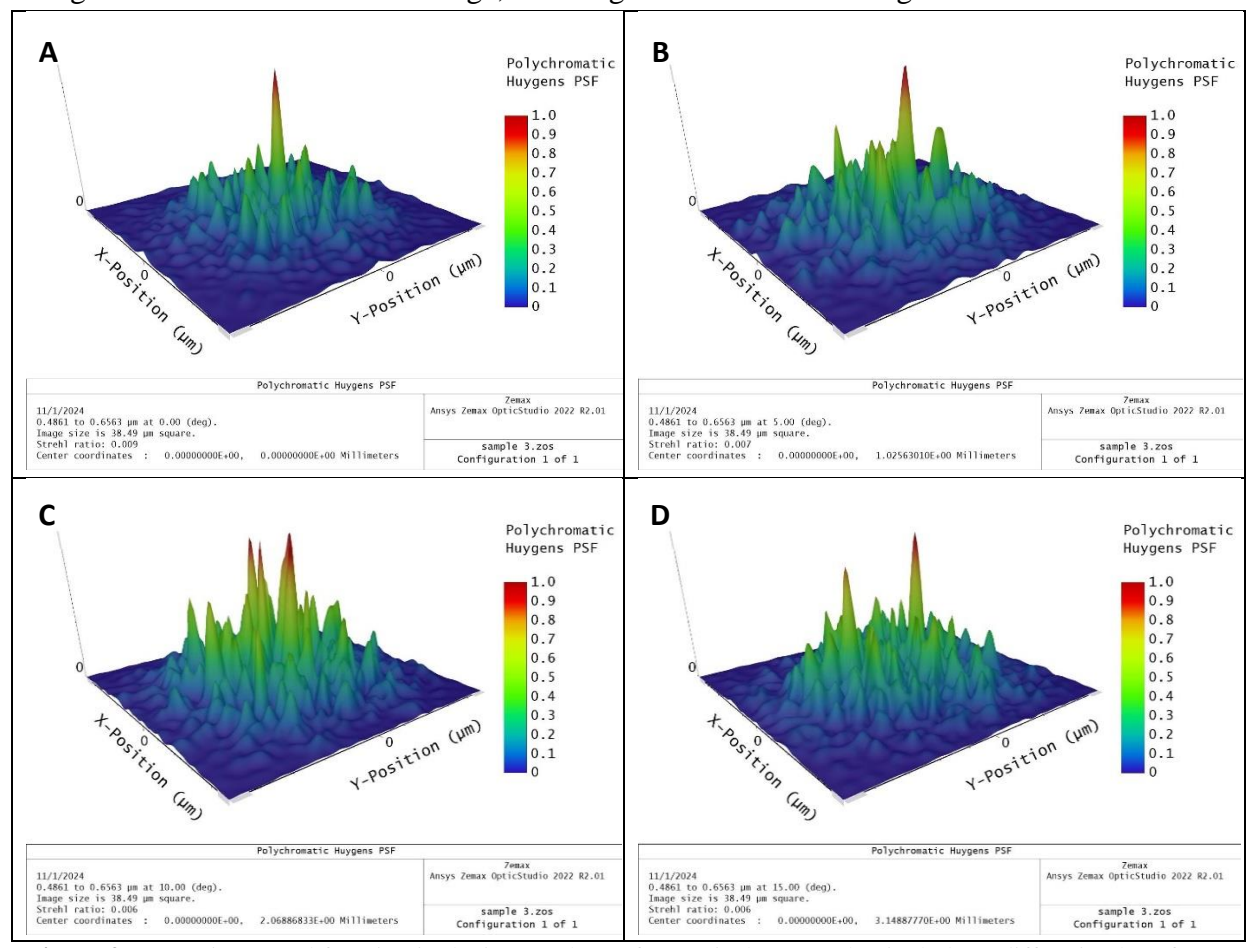


**Figure 2.** 3-D point spread function in the image plane of an optical system that includes a diffractive lens for different values of the incidence angle.

The spot diagram gives a macroscopic picture of the ray distribution in the image plane, especially for a point object, to facilitate comparison with the ideal case. **Figure 3** shows the spot diagram in the image plane for the optical system used for different values of the angle of incidence.

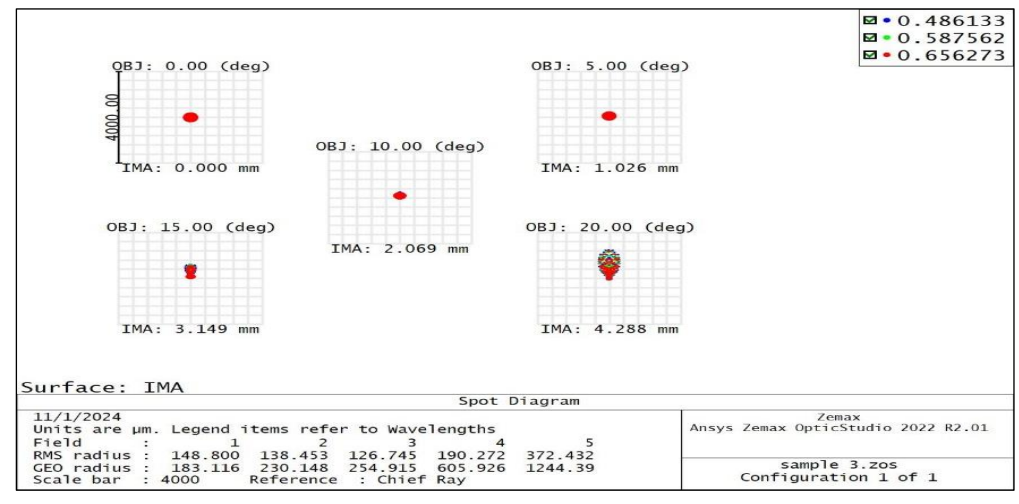


**Figure 3.** Spot diagram of an optical system that includes a diffractive lens for different values of the incidence angle.

The figure shows a change in the shape of the ray distribution as the angle of incidence changes due to the appearance of aberration. The image gradually flattens to a conical shape due to the appearance of non-isotropic comet aberration. The area of the ray spread in the image plane increases with increasing angle of incidence due to the increase in the amount of aberration.

The ray fan aberration diagram shows the amount and type of aberration present in an optical system. It appears as fan-shaped curves on the tangential and sagittal (x and y) image axes. The appearance of the curve in this form results from the incidence of rays on the image plane along the two axes. It starts at the image center and bends in perpendicular directions. The amount and type of curvature determine the amount and type of aberration occurring in the optical system. **Figure 4** shows the aberration diagram in the image plane for an optical system that includes a diffractive lens. The amount of curvature of the curves increases as the angle of incidence increases. The diagram also deviates more in the (y) axis as the angle of incidence increases due to the displacement of the source from the y-axis. This shows the asymmetry in the aberration curve for the two perpendicular axes.

The optical path difference OPD shows the change in the optical path of the wavefront after refraction by the two surfaces of the lens compared to the ideal case where there is no aberration. The ideal case for optical path difference is when the wavefront remains spherical, especially if the object is a point shape. If the spherical shape of the wavefront is distorted after refraction due to aberration, the optical path difference becomes more pronounced in the graph as the curve moves away from the sagittal and tangent axes to the image plane (x and y). **Figure 5** shows the optical path difference of an optical system including a diffracting lens for different values of the angle of incidence. The curve starts to move away from the y-axis more as the angle of incidence increases in the y-axis field at the object location.

The optical transfer function (OTF) represents the image contrast with respect to spatial frequency. It is a very useful function for evaluating image quality in both analog and digital optical systems. The modulation optical transfer function MTF can be used for optical systems with a homogeneous medium at both ends of the lens by maximizing the function to a single magnitude. MTF starts at its highest value at low frequencies and then gradually decreases as the spatial frequency of the light source increases. This is ideal. However, in real optical systems, MTF drops sharply with increasing spatial frequency, followed by small secondary peaks that gradually decrease with increasing frequency.

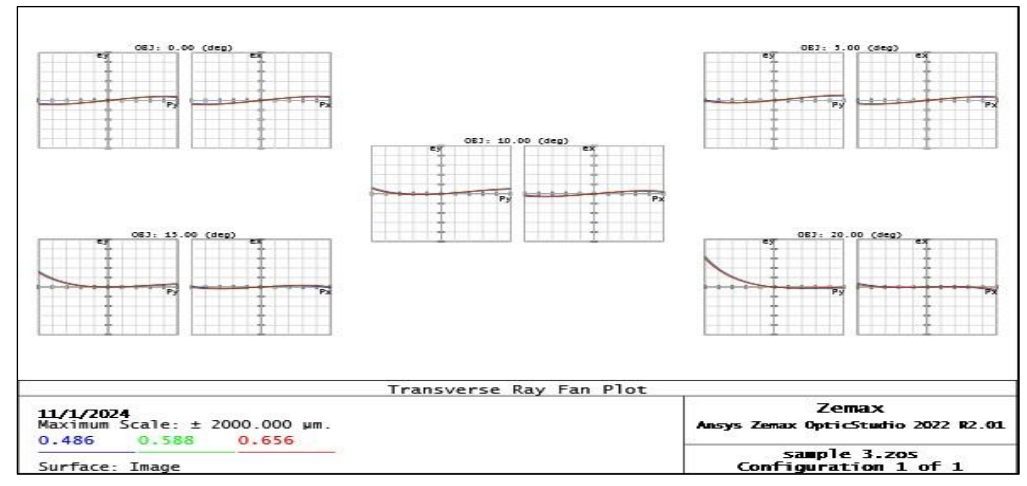


**Figure 4.** Ray fan aberration of an optical system that includes a diffractive lens for different values of the incidence angle.

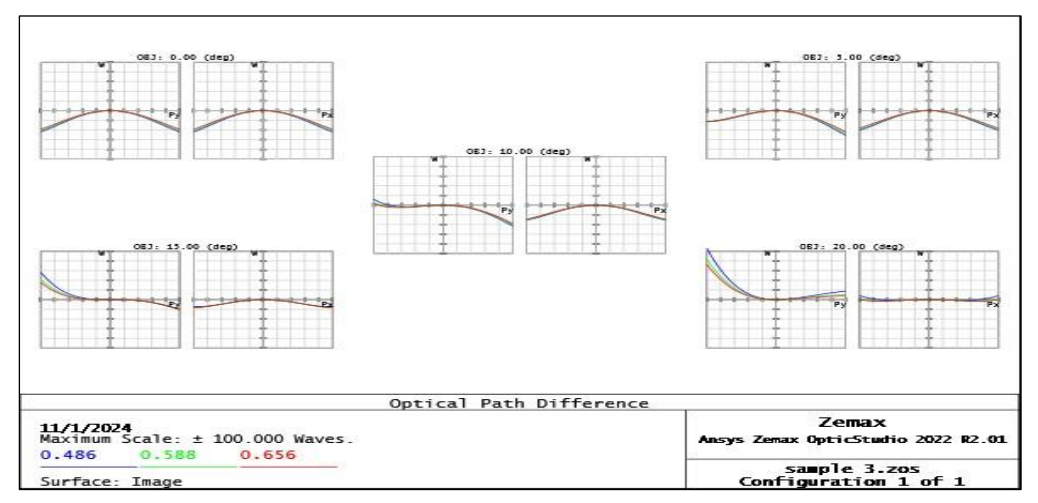


Figure 5. OPD of an optical system that includes a diffractive lens for different values of the incidence angle.

**Figure 6** illustrates the MTF of an optical system used for varying values of the angle of incidence. The figure shows a single curve of the OTF at the angle of incidence (0), meaning that the sagittal and tangential curves of the image axes are identical in this case due to the symmetry of the image. This is not the case in the other figures at different angles; two curves appear in the OTF for the sagittal and tangential axes due to the asymmetry in the image plane.

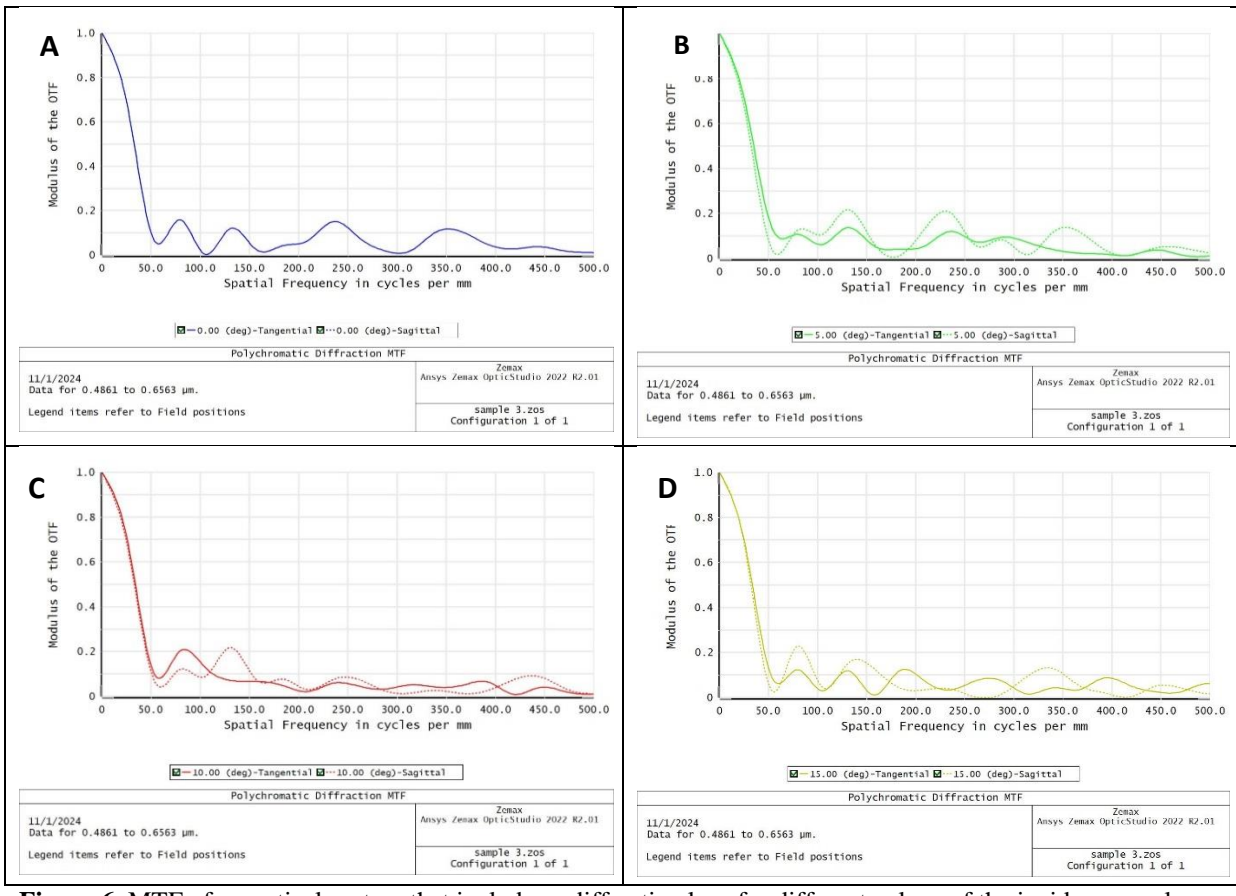
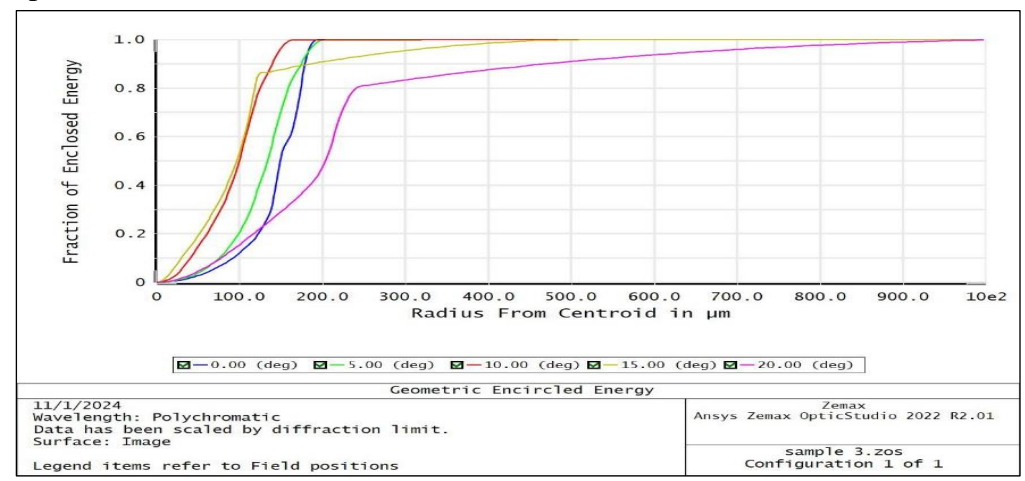


Figure 6. MTF of an optical system that includes a diffractive lens for different values of the incidence angle.

The Encircled energy diagram represents the distribution of the radiant energy of light in the image plane. The image is scanned from the center to the edges in circular or square sectors, depending on the type of function and the image type, whether analog or digital, respectively. The function starts from zero at the origin, as there are no rays at the zero-dimensional point, and then gradually increases with the increase in the scanned area of the image plane along the x-axis of the diagram, which represents the radius of the image plane.

**Figure 7** shows the Encircled energy diagram of an optical system including a diffracting lens for different values of the angle of incidence. The figure shows the curve's increasing distance from the x-axis as the angle of incidence increases. This means that the concentration of rays in the image center decreases as the angle of incidence increases. In other words, the spread of rays in the image plane increases as the angle of incidence increases. This is based on considering the object as a point object. The change in the curve's path results in the appearance of aberration in the image as the object moves away from the optical axis.



**Figure 7.** Encircled energy of an optical system that includes a diffractive lens for different values of the incidence angle.

#### 4.Discussion

The results revealed many specific details about the performance of diffractive lenses compared to conventional lenses and the effects of varying incidence angles and wavelengths. The point spread function (PSF) showed that the diffractive lens produces a diffraction pattern with central and secondary peaks, like conventional lenses. As the incidence angle increases, the intensity of the central peak decreases, and the secondary peaks spread over a larger area, indicating the presence of chromatic aberrations such as spherical aberration, coma, and astigmatism.

The spot diagram showed an increased ray spread in the image plane and asymmetry at large incidence angles, further confirming the degradation of image quality due to chromatic aberration. The aberration plot shows the variation in the value and type of aberration as the incidence angle changes. The deviation of the plot increases as the angle of incidence increases along the y-axis due to the loss of symmetry in the image, making aberrations more pronounced.

MTF shows the change in the path of the wavefront as it passes through the optical system due to reflection or refraction. The specific figures show the increased deviation of the curves as the angle increases due to increased aberration. Regarding MTF and image contrast, results showed that the diffractive lens performed well at low spatial frequencies but exhibited a sharp decrease in contrast at higher frequencies, especially at relatively large angles of incidence. Especially the sagittal and tangent curves at higher angles revealed lens asymmetry and reduced performance in off-axis conditions. This suggests that diffractive lenses are more suitable for applications that do not require high spatial frequency resolution. The encircled energy plots showed that the radiant energy concentration at the image center decreased with increasing angle of incidence, with the energy spreading outward. This indicates a decrease in image sharpness and intensity, which is consistent with other results.

The results indicate that diffractive lenses do not have high image quality in systems with large peripheral light sources.

The results indicate that diffractive lenses produce lower-quality images compared to conventional lenses, particularly in terms of intensity distribution and aberration control. However, their unique properties, such as their lightweight design and flexible slit arrangement, make them suitable for specific applications, such as non-imaging optical systems (such as light alignment or focusing) where high image resolution is less important. The results highlight the importance of carefully selecting optical parameters, such as pupil diameter, lens curvature, and material, to optimize the performance of diffractive lenses. Although diffractive lenses exhibit limitations in system performance in image generation, their unique properties and design flexibility make them a valuable tool in specialized optical systems. The study provides a foundation for future work aimed at improving their performance and expanding their scope of application.

#### 5. Conclusion

A diffractive lens produces a low-quality image compared to a conventional lens, with a marked weakness in the intensity values extracted at the image plane. Furthermore, aberration is evident in an optical system containing a diffractive lens, especially when the angle of incidence increases, and the source is displaced off the optical axis. Therefore, an optical system containing a diffractive lens can be used to a limited extent in imaging optical systems, and extensively in non-imaging optical systems, such as focusing or collimating light rays.

#### Acknowledgment

I extend my thanks to the College of Education for Pure Science, Ibn Al-Haitham, and the University of Baghdad for assisting in completing this work by opening private laboratories and providing scientific facilities by the staff of the Physics Department to help support the research project.

#### **Conflict of Interest**

Alaa B. Hasan declares that he is a member of IHJPAS editorial board at the time of submitting the manuscript. The editor-in-chief of IHJPAS confirms that (Alaa B. Hasan) was excluded from any decisions made regarding this article.

#### **Funding**

None.

#### References

- 1. Khaligh OC, Alireza S. Energy harvesting: solar, wind, and ocean energy conversion systems. CRC press. 2017;22:12-23. https://doi.org/10.1201/9781439815090
- 2. Heidari N, Pearce JM. A review of greenhouse gas emission liabilities as the value of renewable energy for mitigating lawsuits for climate change related damages, Renew. Sustain. Energy Rev. 2016;55(2):899–908. <a href="http://dx.doi.org/10.1016/j.rser.2015.11.025">http://dx.doi.org/10.1016/j.rser.2015.11.025</a>
- 3. Ginley NR, Green A. Solar Energy Conversion Toward 1 Terawatt, Hornessing Mater. Energy. 2008;12(3):355–364. http://dx.doi.org/10.1557/mrs2008.71
- 4. Irena A. Renewable Energy Cost Analysis Concentrating Solar Power. Int Renew. Energy Agency Renew. 2012;23:1–41.
- 5. Rauschenbach S, Hans S. Solar cell array design handbook: the principles and technology of

- photovoltaic energy conversion. Springer Sci Bus Media .2012.
- 6. Dudley E, Kolb J, Mahoney A, Mancini T, Kearney D. Test results: SEGS LS-2 solar collector. Sandia National Laboratory. Albuquerque, NM (United States). 1994;140:33-45.
- 7. Duffie WB, John A. Solar engineering of thermal processes. Appl. Opt. 2013;12: 55-67. <a href="https://DOI:10.1002/9781118671603">https://DOI:10.1002/9781118671603</a>.
- 8. Zhang JX, Hoshino K. Optical molecular sensing and spectroscopy. Optic Transduc. 2019;12(2): 23-45. <a href="http://dx.doi.org/10.1016/B978-0-12-814862-4.00005-3">http://dx.doi.org/10.1016/B978-0-12-814862-4.00005-3</a>.
- 9. Yoneda N, Miyazaki M, Matsumura H, Yamato M. A design of novel grooved circular waveguide polarizers, IEEE Trans. Microw. Theory Tech. 2000;48:2446–2452. <a href="https://doi.org/10.1109/22.898996">https://doi.org/10.1109/22.898996</a>.
- 10.Karp JH, Ford JE. Planar micro-optic solar concentration using multiple imaging lenses into a common slab waveguide, High Low Conc. Syst. Sol. Electr Appl IV. 2009;74(4):70-76. http://dx.doi.org/10.1117/12.826531.
- 11.Karp JH, Tremblay EJ, Ford JE. Radial coupling method for orthogonal concentration within planar micro-optic solar collectors. Opt InfoBase Conf Pap. 2010;12:9–11. <a href="https://doi.org/10.1364/">https://doi.org/10.1364/</a> /OSE.2010.STuD2
- 12. Cheng YL. Review on Optical Waveguides. Shankar, Intech. 2018;11(2):13-18. <a href="https://dx.doi.org/10.5772/intechopen.77150">https://dx.doi.org/10.5772/intechopen.77150</a>.
- 13.Bauser HC. Photonic Crystal Waveguides for >90% Light Trapping Efficiency in Luminescent Solar Concentrators. ACS Photonics. 2020;7:2122–2131. <a href="http://dx.doi.org/10.1021/acsphotonics.0c00593">http://dx.doi.org/10.1021/acsphotonics.0c00593</a>
- 14. Rühle S, Greenwald S, Koren E, Zaban A. Optical waveguide enhanced photovoltaics. Opt Express. 2008;16(2):26-32. http://dx.doi.org/10.1364/OE.16.021801.
- 15. Wang YM, Zheng G, Yang C. Characterization of acceptance angles of small circular apertures. Opt. Express. 2009;12(3):45-56. https://doi.org/10.1364/oe.17.023903.
- 16.Murphy F, Tommy D. Analysing curved optical waveguides using the finite difference beam propagation method. Appl Opt. 2020;11(2):67-78. <a href="https://cora.ucc.ie/items/4ddac268-7e69-42ff-bb8c-74ae144c5b5f">https://cora.ucc.ie/items/4ddac268-7e69-42ff-bb8c-74ae144c5b5f</a>.
- 17.Farhan M, Adnan BI. The effect of temperature on polymethyl methacrylate acrylic (PMMA). Appl Opt. 2013;17:22-34. <a href="https://doi.org/10.1016/j.polymertesting.2016.12.016">https://doi.org/10.1016/j.polymertesting.2016.12.016</a>
- 18.Hsu MY, Shenq TC, Ting MH. Thermal optical path difference analysis of the telescope correct lens assembly. Adv Opt Technol. 2012;6(4):447-453. <a href="https://doi.org/10.1515/aot-2012-0058">https://doi.org/10.1515/aot-2012-0058</a>
- 19. Mahajan VN. Optical Imaging and Aberrations. Ray Geometrical Optics, Part I, II, By SPIE: Press Monograph. 1998;45:344-355. https://doi.org/10.1117/3.265735
- 20.Sanyal S, Ajay G. The factor of encircled energy from the optical transfer function. J Opt A: Pure Appl Opt. 2002;4:208-211. https://DOI.10.1088/1464-4258/4/2/316
- 21.Al-Saadi TM, Hussein BH, Hasan AB, Shehab AA. Study the structural and optical properties of Cr doped SnO<sub>2</sub> nanoparticles synthesized by sol-gel method. Energy Proc. 2019;157:457–465. https://doi.org/10.1016/j.egypro.2018.11.210
- 22. Alaa BH, Husain SA. Design of Light Trapping Solar Cell System by Using Zemax Program. <u>J</u> Phys: Conf Series. 2018;1003:25-32. https://DOI.10.1088/1742-6596/1003/1/012074
- 23.Alaa BH. Studying Optical Properties of Quantum Dot Cylindrical Fresnel Lens. NeuroQuantology 2022;20(2):97–104. http://dx.doi.org/10.14704/nq.2022.20.1.NQ22013
- 24.Hamza HN, Alaa BH. Design of Truncated Hyperboloid Solar Concentrator by Using Zemax Program. Ibn Al-Haitham J Pure Appl Sci. 2022;35(2):1-7. <a href="http://dx.doi.org/10.30526/35.1.2780">http://dx.doi.org/10.30526/35.1.2780</a>
- 25.Al-Hamdani AH, Rashid HG, Hasan AB. Irradiance distribution of image surface in microlens array solar concentrator. ARPN J Eng Appl Sci. 2013;5:23-31.
- 26.Karszewski KM, Stewen C, Giesen A, Huge H. Theoretical modeling and experimental investigations of the diode-pumped thin-disk Yb :YAG laser, Quantum Electron. Optica Mag. 1999;29:86-97. https://DOI.10.1070/QE1999v029n08ABEH001555
- 27.Mohammad HS. Determination and suppression of back reflected pump power in Yb:YAG thin-disk laser. Optical Eng. 2017;56(1):1-8. <a href="http://dx.doi.org/10.1117/1.OE.56.2.026109">http://dx.doi.org/10.1117/1.OE.56.2.026109</a>

- 28. Hariton V. Feasibility study and simulation of a high-energy diode-pumped solid-state amplifier. Tecnico Lisboa. 2016;12(3);1-94.
- 29.Kazemi SS, Mahdieh MH. Determination and suppression of back-reflected pump power in Yb:YAG thin-disk laser. Optical Eng. 2017;56:026109. http://dx.doi.org/10.1117/1.OE.56.2.026109
- 30.Khudair YY, Alaa BH. Design and Evaluation of Polygonal Trough Solar Concentrator. Ibn Al-Haitham J Pure Appl Sci. 2021;34(4):10-16. http://dx.doi.org/10.30526/34.4.2696